A Periodic Density Functional Theory Analysis of CO Chemisorption on Pt(111) in the Presence of Uniform Electric Fields†

P. Deshlahra,‡ E. E. Wolf,‡ and W. F. Schneider*,‡,§

Department of Chemical and Biomolecular Engineering and Department of Chemistry and Biochemistry, University of Notre Dame, Notre Dame, Indiana 46556

Received: November 30, 2008; Revised Manuscript Received: February 13, 2009

Periodic DFT calculations are used to study the effect of a homogeneous electric field applied perpendicular to a Pt(111) surface on the bond distances, binding energies, and vibrational frequencies of atop- and fcc-adsorbed CO at various coverages. The observed structural and energetic modifications can be understood in terms of modest field-induced charge transfer between charged metal surface and adsorbate and are well-described by classical first and second-order Stark models. Electronic differences between atop and fcc adsorption cause CO in these sites to respond differently to applied fields. After correcting for the GGA site preference error, CO adsorption is predicted to shift from atop to fcc at potentials < -0.19 V Å^{-1}. The results are in qualitative agreement with previously reported cluster-based DFT models but differ quantitatively due to difference in modeled coverage, surface relaxation, and finite size effects. The calculated 44.4 cm^{-1} V^{-1} Å shift in C−O stretch frequency with electric field (Stark tuning rate) compares favorably with UHV experiments but is significantly lower than the value obtained in electrochemical measurements, highlighting the importance of adsorbate environment on the magnitude of the tuning rate. The calculated coverage dependence of the tuning rate is in good agreement with previous UHV experiments.

Introduction

Imposed or intrinsic electrostatic fields can have a significant effect on the chemisorption of molecules at metal surfaces and thus are important in a number of physical systems related to electrochemistry and catalysis. Thus, an understanding of the fundamental electronic processes contributing to and controlling field effects is important. Carbon monoxide (CO) adsorbed on Pt(111) is a well-known model for molecular chemisorption on metal surfaces[1] and has been studied extensively for both gas-phase and electrochemical systems. CO adsorption on Pt(111) presents well-known challenges to standard generalized gradient approximation (GGA) implementations of density functional theory (DFT),[2] making this an excellent candidate for detailed analysis of the intereaction between surface electronics and electric field.

The electrochemical double layer (EDL) at the metal-solution interface is characterized by excess charge density in the metal and counter charge in the solution, leading to strong electric fields at the interface. Experimental techniques such as in situ vibrational spectroscopy can provide important information about the nature of chemisorption at such interfaces. For example, a change in the vibrational frequency of adsorbates with changing electric field, called the vibrational Stark effect, has been studied extensively for C−O on different metal electrodes.[3−6] In these studies a change in C−O stretch vibrational frequency is recorded as a function of electrode potential ϕ. Some assumptions about the double layer are required to calculate the rate of change of vibrational frequency with electric field, $d\nu/dF$, from the measured $d\nu/d\phi$ data. A common approach is to assume that the potential drop is located entirely within the Helmholtz double layer and the field inside this layer is uniform. For an electrode potential of 3 V the strength of electric field can be up to 1 V Å^{-1}. These studies show that an external potential has a significant effect on chemisorption at electrochemical interfaces, including a change in preferred CO adsorption site from atop to hollow on a Pt electrode.[3]

Using a combination of reflection absorption spectroscopy (RAIRS) and electro-reflectance vibrational spectroscopy (EVS), Luo et al. measured the Stark tuning rate for CO adsorbed on Pt(111) and other metal surfaces in a UHV environment at different coverages.[7] They found that the magnitude of Stark tuning decreases linearly with coverage due to increased screening of the external electric field by the adsorbates. The vibrational Stark effect was explained by Lambert using a semiclassical model that included an empirical screening factor, γ, which relates the applied external electric field to the local electric field near the adsorbate dipole. This screening factor was shown to vary linearly with coverage. The Stark tuning rates calculated from these UHV experiments are qualitatively in agreement with the electrochemical results but have about half the magnitude. The reason for this difference was explained by Lambert to be due to different screening factors in these two environments.

Although not as directly evident as the electrochemical and UHV systems described above, electric fields can have significant effects on adsorption energies and reaction rates in heterogeneous catalytic systems. Promoters and coadsorbed ions on metal surfaces are known to alter catalytic activity and selectivity toward chemical reactions. Ab initio electronic structure calculations suggest that these ions create long-range electrostatic interactions[8,9] that are similar to a uniform external electric field.[8] Electric field effects are also important to the interface between dispersed metal particles and semiconductor supports. Charge transfer from the support to the metal can lead

† Part of the "George C. Schatz Festschrift".

* Corresponding author. E-mail: wschneider@nd.edu.
‡ Department of Chemical and Biomolecular Engineering.
§ Department of Chemistry and Biochemistry.

10.1021/jp810518x CCC: $40.75
Published on Web 03/11/2009

to strong electric fields at metal sites near the interface. This effect, first proposed by Schwab[10] and later termed the Schwab effect of the second kind, has often been identified as a possible reason for the modification of catalytic activity in supported catalysts.[11,12] A theoretical study electric field effects can improve our understanding of the nature of this phenomenon.

Chemisorption in the presence of an applied external electric field and the vibrational Stark effect have been studied for a number of adsorbates on metal surfaces using finite cluster models of the metals.[3,13−16] The main aim of most of these studies was to simulate the effect of the EDL at an electrode surface. Although these studies provided useful insights about the nature of the effect of external electric field on chemisorption, in many cases the results were strongly dependent on the choice of physical model parameters, such as metal cluster size.[16,17]

More recently, calculations on metal-adsorbate systems in an electric field have been performed using DFT and a slab model within a periodic supercell. External electric fields have been implemented using three different approaches. In the first approach, electrons are injected into or removed from the metal slab and a uniform background electrostatic charge of the same magnitude and opposite sign is introduced to maintain the overall electrical neutrality of the cell.[18,19] In this method the electric field in the vacuum region decreases linearly with distance from the metal surface. This method has been used by Taylor et al. to vary the potential in electrochemical surface simulations.[19] In the second approach, electrons are again added or removed from the slab, but here electrical neutrality is maintained by introducing a sheet of compensating charge in the middle of the supercell vacuum region.[20−22] This configuration generates a uniform electric field between the metal slab and charge sheet, symmetric on both sides of the slab. The final approach, first proposed by Neugebauer and Scheffler, does not need addition or removal of electrons from the supercell. Instead, a dipole sheet is introduced in the middle of the vacuum region that polarizes the periodic slab and imposes a uniform electric field of opposite sign on either side of the slab.[23,24] In each of the above models the electric potential distribution in the vacuum region can be derived from classical electrostatics and is governed by Poisson's equation,

$$\nabla^2\phi = -\frac{\rho}{\varepsilon_0} \tag{1}$$

where ρ is charge density and ε_0 is the permittivity of free space. The electric field F is related to the potential by

$$F = -\nabla\phi \tag{2}$$

The boundary conditions for Poisson's equation over the vacuum region is provided by the electric fields at the surfaces of the slab,

$$F_{\text{surface}} = \frac{\sigma}{\varepsilon_0} \tag{3}$$

where σ is the surface charge density. Figure 1 shows schematic representations of the above three methods and corresponding potential distribution compared to a supercell with no external potential or field. The uniform background charge density ρ in Figure 1b leads to a decaying slope of electrostatic potential and hence a decaying electric field. In Figure 1c,d, ρ is zero, creating a linear variation in potential and a uniform electric field.

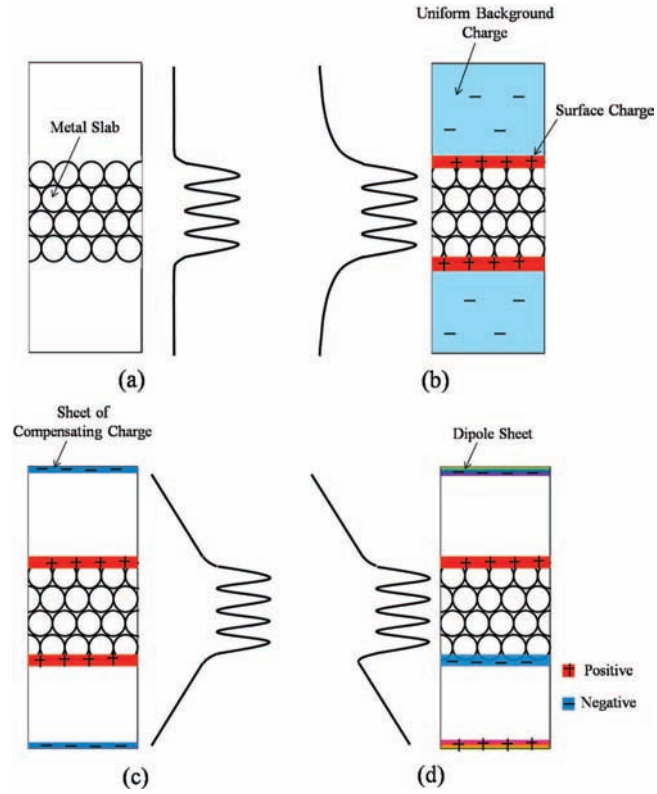

Figure 1. Schematic comparison of different methods of imposing an electric field in periodic supercell calculations and corresponding potential variation in the supercell. (a) shows a slab without any imposed field for comparison.

Recent comparisons have shown significant differences between finite cluster and periodic supercell models for electric field dependent chemisorption. Hyman and Medlin[16] studied the effect of electric field on oxygen chemisorption and dissociation on Pt(111) using both cluster and slab approaches. They found that the energy changes due to applied electric field were about an order of magnitude smaller in the slab calculations. Lozovoi and Alavi studied the vibrational Stark effect on atop-adsorbed CO on Pt(111) using a periodic model[21] and found the magnitude of the shift in vibrational frequency to be much smaller in the latter. More recently, Curulla Ferré and Niemantsverdriet examined the vibrational Stark effect on the same model surface and showed that the tuning rate is insensitive to adsorption site and is screened at increasing coverages.[25] These periodic calculation results were closer to the UHV results whereas the cluster calculations favored the electrochemical ones. The above studies have quantified the vibrational Stark effects but leave open questions of its electronic origins.

The GGA is well-known to overestimate CO adsorption energies and to incorrectly predict CO to prefer 3-fold hollow over atop adsorption on Pt(111). Feibelman et al.[2] showed that this error is common to all GGA implementations. For instance, the RPBE functional[26] improves the adsorption energy at the expense of less accurate lattice constants and surface energies but does not correctly predict the site preference. The origin of the problem has been traced to an underestimation of the CO HOMO−LUMO gap in the GGA.[27,28] Kresse et al.[28] showed that by varying the CO $2\pi^*$ orbital energy by using a GGA + U Hubbard model, it is possible to recover the experimentally

observed atop preference. Mason et al.[29] similarly observed a correlation between site preference and HOMO−LUMO gap and showed that the experimental preference could be recovered by extrapolating the CO singlet−triplet excitation energy vs binding energy correlations to the experimental CO singlet−triplet excitation value. To date, the effects of these corrections on field-dependent CO adsorption have not been explored.

In the present study we use the dipole sheet method of Neugebauer and Scheffler to analyze the effect of applied field on CO chemisorption electronics, energetics, bond lengths and vibrational frequencies on Pt(111). We calculate adsorbate dipole moments and polarizabilities by integration of calculated charge densities vs applied field and show that these two parameters govern the electric field dependence of the adsorption energies. We analyze the differing field dependences of CO adsorption in atop and hollow sites and, by correcting the zero field adsorption energies using the extrapolation method proposed by Mason et al.,[29] predict the atop−fcc site preference difference as a function of field. We show that electric field effects on various properties exhibit trends similar to the previously reported cluster-based calculations, but that the magnitudes of the dipole moment, polarizability, and vibrational Stark tuning rates are significantly different because of the limitations of the cluster model. The present periodic calculations predict Stark tuning rates closer to those measured in UHV experiments than the cluster calculations and also explain the coverage dependence.

Computational Details

DFT calculations were performed using the periodic supercell plane-wave basis approach, as implemented in the VASP[30] code. Atom cores were described with the projector augmented wave (PAW)[31,32] method, and plane waves were included to an energy cutoff of 400 eV. Electronic energies were computed with the PW91 implementation of the generalized gradient approximation (GGA).[33,34] Ionic iterations were performed until the forces on the ions were less than 0.002 eV Å^{-1}. A Gaussian smearing profile with a smearing parameter of 0.10 eV was imposed at the Fermi level, and energies were extrapolated to zero smearing.

The bulk Pt lattice constant was calculated within a primitive face-centered-cubic (fcc) cell using a 10 × 10 × 10 Monkhorst−Pack **k**-point mesh. The Pt(111) surface was represented by a four-layer-thick slab separated by a four layer vacuum space. Atoms in the two middle layers were fixed at their bulk locations whereas the top and the bottom layers were allowed to relax. Calculations were performed for a bare slab and with one CO adsorbed at the experimentally observed atop site and the DFT-preferred 3-fold fcc site. The majority of calculations are performed within a 2 Pt × 2 Pt supercell, yielding $^1/_4$ monolayer coverage (Figure 2). A 6 × 6 × 1 Monkhorst−Pack[35] **k**-point mesh was used for numerical integration over the Brillouin zone. Some calculations were performed with a coarser **k**-point mesh to estimate the effect of **k**-point sampling on trends observed with electric field. To study the effect of coverage on atop-adsorbed CO, calculations were also performed on three Pt × 3 Pt and 4 Pt × 3 Pt supercells, corresponding to a $^1/_9$ and $^1/_{12}$ monolayer CO coverages respectively. A 3 × 3 × 1 Monkhorst−Pack **k**-point mesh was used for these calculations. To study the effect of surface relaxation, some calculations were performed with all Pt atoms fixed to their bulk positions. The gas-phase CO molecule was simulated in a cubic supercell 20 Å on a side, large enough to ensure negligible interaction between neighboring cells.

An external electric field perpendicular to the slab was imposed using the method proposed by Naugebeaur and Scheffler[23] as implemented in VASP.[24] In this method, a planar dipole layer, consisting of point charges, is introduced in the vacuum to correct for the interaction between an adsorbate-induced surface dipole and its periodic images along the surface normal. The magnitude of dipole moment of the planar dipole layer can be determined self-consistently to cancel out spurious interactions between periodic images, but it can also be specified explicitly to introduce a true external electrostatic field (Figure 1d). For the case of no external field, calculations were performed both with and without the dipole correction. Because CO has a small dipole moment, this zero-field dipole correction has a negligible effect on structures and energies. The maximum electric field that can be introduced is limited by the height of the supercell, as described below. The supercell dimensions used in this work allowed use of electric fields up to ±1 V Å^{-1}. A negative electric field corresponds to accumulation of electrons on the CO-adsorbed side of the slab and its depletion on the other side. To determine the effect of applied electric field on the binding energy of a CO molecule that arrives from outside the field, total energies were calculated for gas-phase CO without an applied field and for the bare and CO-adsorbed slabs in the applied field. The adsorption energy is defined as:

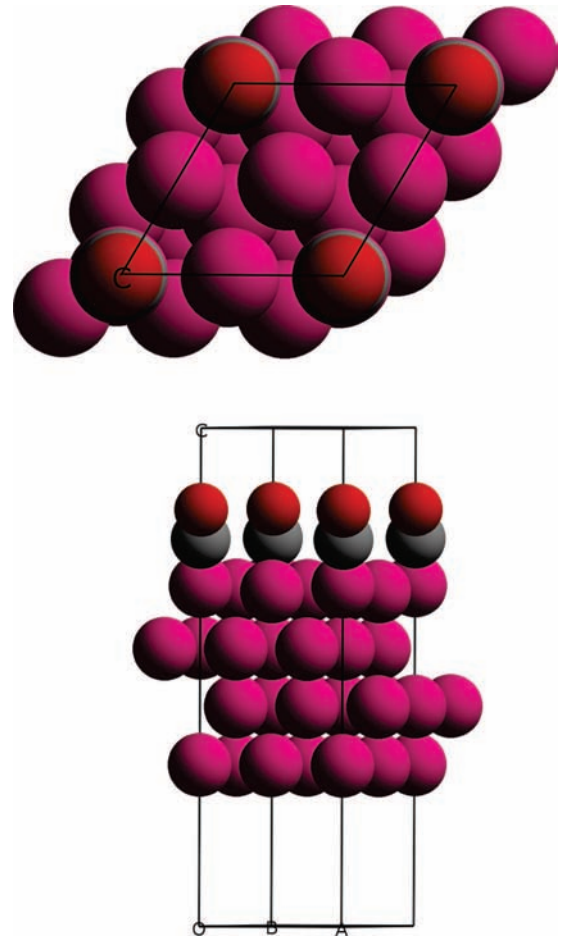

Figure 2. Pt(111) slab with four Pt atom layers and $^1/_4$ monolayer CO coverage used for periodic DFT calculations.

$$\Delta E_{ads} = E^{DFT}_{Pt-CO} - E^{DFT}_{Pt} - E^{DFT}_{CO} \quad (4)$$

As described below, corrections for the GGA underprediction of the CO $5\sigma-2\pi^*$ gap are obtained by calculating field-dependent adsorption energies with three different PAW models.

TABLE 1: Bond Lengths and Vibrational Frequencies of Atop CO on Pt(111) at Zero Electric Field Estimated from Various Cluster and Periodic Calculations

θ (monolayers)	r_{Pt-C} (Å)	r_{C-O} (Å)	ν_{Pt-C} (cm^{-1})	ν_{C-O} (cm^{-1})	ref
		Cluster Calculations			
0	1.90	1.154		1987	3
0	1.90	1.159	408	2000	13 and 14
0	1.86	1.158			27
0	1.907	1.152	409	2098	46
0	1.830	1.166	505	2000	47
		Periodic Calculations			
0.0625	1.862	1.157	510	2054	47
0.11	1.878	1.155			27
0.25	1.88	1.15		2120	48
0.25	1.855	1.152	495	2033	21
0.25	1.845	1.158	514	2072	25
0.33	1.878	1.155			27
0.083	1.854	1.156	508	2064	present
0.25	1.851	1.157	504	2076	present

A 700 eV cutoff is used for the smallest-core models. CO triplet excited-state energies are calculated including spin polarization. All the other computational details remain the same.

Vibrational frequencies were calculated by diagonalization of the dynamical matrix, constructed using two-sided finite differences on the GGA gradients. C, O, and its immediate neighbor Pt atom were included in the finite differences and were perturbed in turn along three orthogonal directions by ±0.02 Å.

The dipole moments are calculated by numerically integrating the charge density multiplied by the position vector over the supercell volume. Dipole moments of adsorbed CO molecule reported are the difference between the dipole moment of the Pt slab with adsorbed CO and that of the bare Pt slab. The polarizability value is the slope of this dipole moment difference vs electric field curve.

Results and Discussion

Field-Dependent Adsorption Electronics. An equilibrium lattice constant of 3.986 Å and bulk modulus of 2.604 Mbar were found from bulk Pt calculations. These values are in good agreement with experimental data.[36] The calculated lattice constant exceeds the experimental value of 3.92 Å by about 2%, which is in agreement with previous reports[2] and consistent with the general tendency of GGA to overestimate intermolecular distances. The Pt(111) surface energy was found to be 1.3 J m^{-2}, which is also in agreement with other models.[37]

The calculated gas-phase C−O bond length and dipole moment are calculated to be 1.142 Å and 0.029 e Å, respectively, which only slightly overestimate the experimental values of 1.128 Å[38] and 0.023 e Å.[39] The positive dipole moment implies a $C^{\delta-}O^{\delta+}$ charge distribution. Table 1 compares the calculated zero-field atop CO Pt−C and C−O equilibrium bond lengths and vibrational frequencies from this work with previous theoretical results. The C−O bond length is in good agreement across different studies whereas the Pt−C distance tends to be slightly smaller in periodic calculations compared to cluster ones. The vibrational frequencies are more sensitive to details of the theoretical model and are more scattered across different studies.

To analyze the effect of electric field on the distribution of electrons and the electrostatic potential inside the supercell, the electronic charge density difference $\Delta\rho(z)$ and electrostatic potential difference $\Delta\phi(z)$ between a neutral slab and a slab with a −1.0 V $Å^{-1}$ applied electric field were calculated and averaged in the directions parallel to the surface plane:

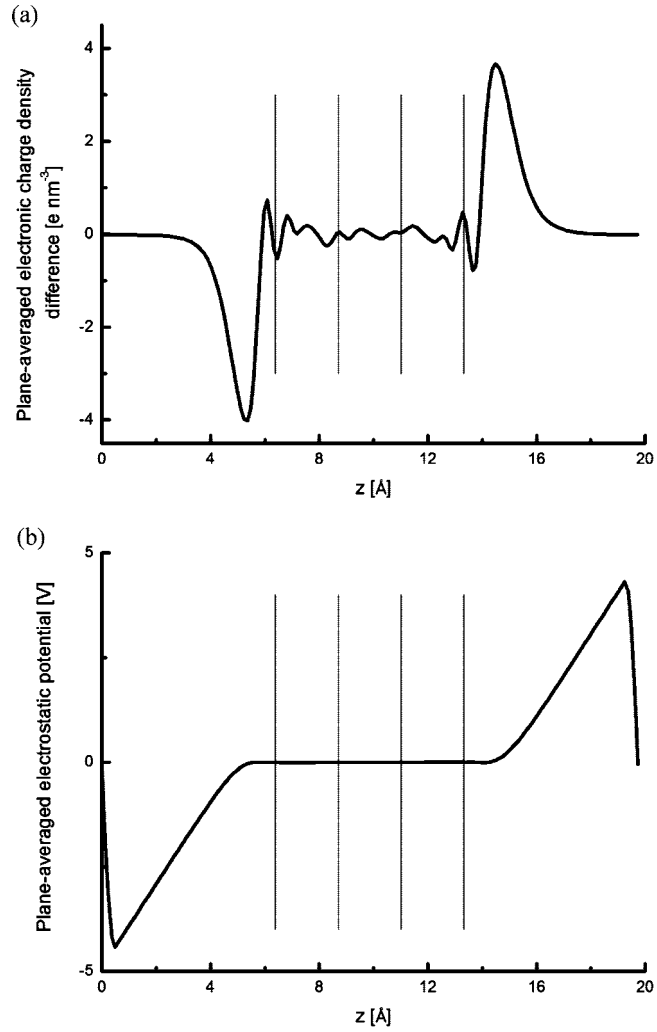

Figure 3. Plane-averaged (a) electronic charge density difference and (b) electrostatic potential difference between a bare four-layer Pt slab calculated with no external field and in a −1.0 V $Å^{-1}$ field. Vertical lines represent the positions of the Pt layers.

$$\Delta\rho(z) = \frac{1}{A}\int_A [\rho_{field}(x,y,z) - \rho_0(x,y,z)]\,dx\,dy \qquad (5)$$

$$\Delta\phi(z) = \frac{1}{A}\int_A [\phi_{field}(x,y,z) - \phi_0(x,y,z)]\,dx\,dy \qquad (6)$$

where A is the area of cross-section and ρ_{field}, ϕ_{field}, ρ_0, and ϕ_0 are charge densities and electrostatic potential inside the supercell with and without applied electric field, respectively. Figure 3 shows the charge and potential differences for a bare slab without any CO adsorbed. The vertical lines denote the positions of the Pt atom layers. Charge accumulation on one side and depletion from the other side of the slab can be seen. The calculated charge accumulation in an electric field of −1.0 V $Å^{-1}$ is 5.5×10^{-3} e $Å^{-2}$, or 0.04 electrons per surface Pt atom, which is identical to that predicted from classical electrostatics by eq 3. As expected for a metal, except for small oscillations, there is no charge accumulation inside the metal and the applied external field is completely screened by surface

charge. The strength of the electric field can be observed as the negative of the slope of the electrostatic potential distribution in the straight-line region (eq 2). The sharp change in potential at the edge of the supercell is due to the dipole sheet introduced in the cell to impose the electric field. It can be seen that for this field strength of -1.0 V Å^{-1}, the potential drop from the surface of the slab to the edge of the supercell is around 4.5 V. For stronger electric fields the potential drop will be steeper. If the potential difference between the slab edge and the supercell edge becomes greater than the work function of the slab, electrons will escape from the surface and some electron density will be found near the edge of the supercell. This puts an upper limit on the strength of the electric field that can be introduced in the calculations. Clearly, the same potential drop can be imposed by increasing the field and decreasing the supercell size in the z direction, but the cell must be thick enough to prevent overlap between the atomic electronic density and the dipole sheet.

Electric-field-induced charge accumulation occurs at the outer surfaces of the slab with no change in charge density at the Pt centers. When a CO molecule is adsorbed on the slab, the charge density distribution responds by spreading further to the adsorbate. Figure 4 shows the electronic charge density and potential distributions in response to a -1.0 V Å^{-1} applied electric field on a slab with atop CO. Distributions for a bare slab are also shown for comparison. It can be seen that charge accumulation occurs not only at the outer region of the O atom but also at the O atom center position (Figure 4a). This result indicates not just an electrostatic redistribution of surface charge in response to a change in geometry but also electron transfer from (or to) the surface to (or from) the adsorbate induced by the electric field.

The Pt−CO bond is generally understood in terms of the Blyholder back-donation model,[40] in which the filled CO 5σ bonding orbital donates charge to vacant metal states and the vacant CO $2\pi^*$ antibonding orbitals accept charge from filled metal d states. The surface charge accumulation or depletion associated with an applied field drives charge into or out of these states, as is evident by shifts of the 5σ and $2\pi^*$ states with respect to the Fermi level and changes in associated orbital occupancy. As shown in Figure 5, a -1 V Å^{-1} applied electric field shifts the atop CO states down in energy relative to the Fermi level, enabling better energy match between CO $2\pi^*$ and Pt d states, increased back-donation, and shortening of the Pt−C and lengthening of the C−O bonds. This charge transfer can be quantified by integrating the angular-momentum-resolved projected density of states (PDOS) up to the Fermi level while holding the geometry constant. The CO σ- and Pt-state occupancies change by less than 0.01 e in a -1 V Å^{-1} field, but the CO π-state occupancies increase by 0.03 e, very close to the 0.04 e/Pt total classical surface charge accumulation noted above. Charge transfer to atop CO is reflected in the CO dipole moment, which we calculate as the difference in dipole between bare and CO-adsorbed slabs. Atop CO has a zero-field dipole moment similar in sign and magnitude to gas-phase CO. Figure 6a shows the negative shift in the dipole moment in negative fields, again corresponding to increased electron accumulation near oxygen atom. Positive electric fields have an effect opposite, decreasing π-state occupancy and increasing the dipole moment (Figure 6a). The slope of the dipole moment corresponds to the polarizability, which we calculate to be 0.151 e Å^2 V^{-1}.

CO adsorbed in an fcc site responds in a congruous way to applied fields. At zero field, fcc CO has greater π and lesser σ

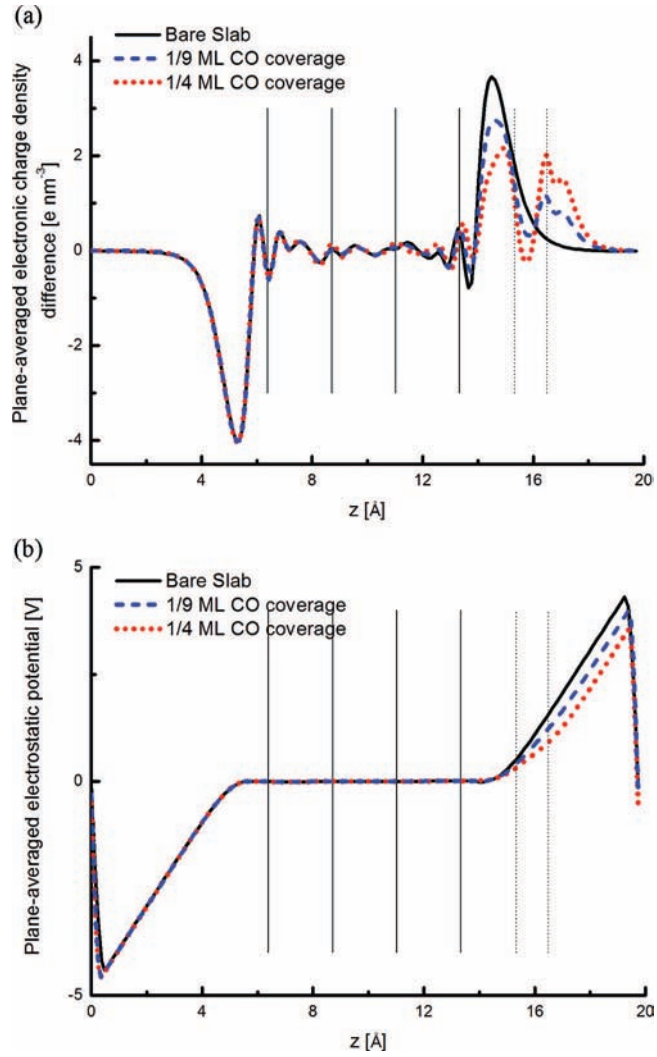

Figure 4. Plane-averaged (a) electronic charge density difference and (b) electrostatic potential difference between no external field and a -1.0 V Å^{-1} field for a bare Pt slab and for Pt slabs with CO adsorbed atop at two different coverages. Solid vertical lines represent the positions of Pt layers and dotted vertical lines represent C and O atoms.

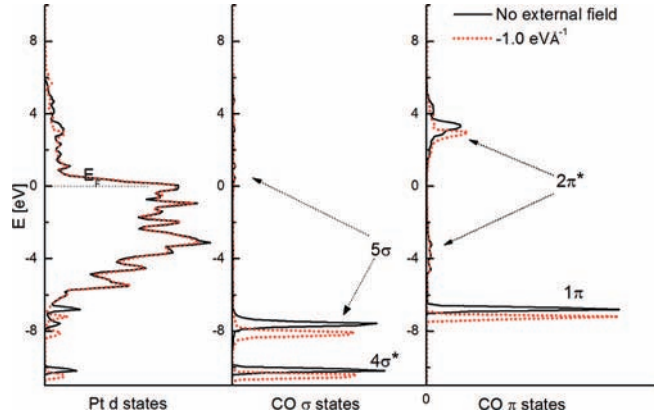

Figure 5. Projected surface Pt and adsorbed atop CO density of states in the absence and presence of applied external field.

occupancies, owing to the better overlap between π and Pt d states in this 3-fold site. The zero-field dipole moment is thus of opposite sign and larger in magnitude than atop CO (Figure 6a). Again, the dipole shifts to more negative values in negative fields, but with a slightly smaller slope than for atop CO. The

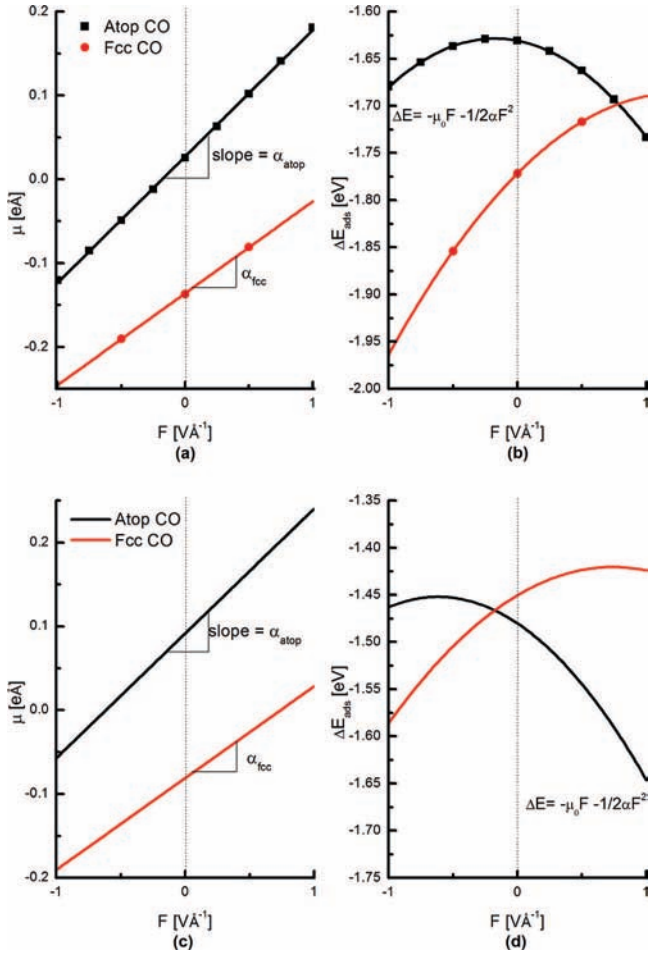

Figure 6. Change in CO dipole moment (left) and adsorption energy (right) at atop and fcc hollow sites with external electric field before (top) and after (bottom) correction of zero field binding energy, dipole moment and polarizability.

fcc polarizability is 0.110 e Å^2 V^{-1}, approximately 30% less than for atop CO. The lower π-state occupancy in atop CO increases the sensitivity of its dipole to applied field.

Field-Dependent Adsorption Energies and Site Preferences. Figure 6b shows the calculated variation in atop- and fcc-bound CO binding energies with applied electric field. The binding energies are calculated to change on the order of several tenths of an electronvolt in response to the fields studied here, and to respond differently depending on site. These trends are well described by a simple electrostatic Stark model. The energy change ΔE due to the interaction of an adsorbate surface dipole with a uniform electric field is given by the first order Stark effect as

$$\Delta E = -\mu_0 F \tag{7}$$

where μ_0 is the adsorbate dipole moment as described above at zero electric field and F is external electric field. The change in dipole moment with applied field is given by

$$\mathrm{d}\mu = \alpha\, \mathrm{d}F \tag{8}$$

where α is the adsorbate polarizability at the surface. This polarization introduces a second-order correction to the interaction of the dipole with the electric field (the second-order Stark effect):

$$\Delta E = -\mu_0 F - \frac{1}{2}\alpha F^2 \tag{9}$$

Figure 6 shows that this model describes the field-dependent binding energies quite reliably. Table 2 summarizes the fitted μ_0, which agree very well with the zero-field adsorbate dipole moments derived by direct integration of the charge densities above, and fitted α, which equal the values calculated from the slopes of the dipole moments in Figure 6a. Thus, dipole moments and polarizabilities derived from surface charge analysis can be used to predict field dependent adsorption energies reliably. Table 2 also compares the fitted μ_0 and α from this work with those obtained by fitting the field-dependent binding energies from previous periodic and cluster calculations to eq 9. Periodic calculations with different GGA functionals lead to very similar electric field effects, whereas cluster calculations predict polarizabilities almost three times larger.

As a consequence of the differing dipole moments and polarizabilities of atop and fcc CO, the energy difference between sites is a strong function of field strength: negative fields favor fcc adsorption whereas positive favor atop (Figure 6b). The observed preference for fcc over atop at zero field is a well-known failing of the GGA[2] that can be traced to an underprediction of the $2\pi^*$ orbital energy and overprediction of backdonation. Mason et al.[29] demonstrated that the energy difference between the ground singlet ($5\sigma^2$) and first excited triplet ($5\sigma^1 2\pi^1$) states of gas-phase CO is a surrogate for this over prediction error, and that the CO adsorption energy (ΔE_{ads}) scales linearly with this singlet−triplet excitation energy ($\Delta E_{s\text{-}t}$). By calculating ΔE_{ads} at different sites vs $\Delta E_{s\text{-}t}$ across a series of GGA norm-conserving pseudopotentials of differing cutoff radii and extrapolating to the experimental $\Delta E_{s\text{-}t}$ value, they were able to recover the experimentally observed preference for atop over multifold adsorption.

Here we apply a similar approach to the electric-field-dependent adsorption energies. We recalculate the adsorption energies at atop and fcc sites in 0, −0.5, and 0.5 V Å^{-1} electric fields using a set of PAW core models differing in cutoff radius and hardness, as described in Table 3. $\Delta E_{s\text{-}t}$ is sensitive to the PAW model, and as shown in Figure 7, the zero-field atop and fcc binding energies do scale nearly linearly with $\Delta E_{s\text{-}t}$. Extrapolating to the experimental $\Delta E_{s\text{-}t}$ value of 6.095,[41] ΔE_{atop} becomes 0.03 eV more negative than ΔE_{fcc}. We calculate binding energies vs applied field using all three PAW models, fit the results of each to eq 9, and extrapolate all the quantities to the experimental $\Delta E_{s\text{-}t}$. Table 4 shows the calculated zero-field adsorption energies and fitted dipole moments and polarizabilities for each core model, along with the extrapolations to the experimental $\Delta E_{s\text{-}t}$. (Extrapolating the field-dependent binding energies to the experimental $\Delta E_{s\text{-}t}$ limit and constructing one fit to eq 9 yields identical results.) The linear correlation coefficients are greater than 0.99 in all cases. As seen in the table, the atop and fcc-adsorbed CO polarizabilities are insensitive to this extrapolation, but the dipole moments of both move toward more positive values in accord with the shift in CO $2\pi^*$ states to higher energy and a concomitant decrease in Pt d to $2\pi^*$ back-donation.

Using the corrected zero-field binding energies, dipole moments, and polarizabilities, we project the field-dependent binding energies to ±1 V Å^{-1} using eq 9. The results are shown in Figure 6d, which can be compared with the uncorrected results in Figure 6b. Atop adsorption becomes preferred over fcc at zero field, but this preference is predicted to reverse at −0.187 V Å^{-1}. This value is quite close to the predicted

TABLE 2: Atop and fcc CO/Pt(111) Adsorption Energies, Zero Field Dipole Moments, and Polarizabilities from Periodic and Cluster DFT Calculations

computational details	ΔE_0 (eV)	μ_0 (e Å)	α (e Å^2 V^{-1})	ref
Atop Site				
periodic, PAW-PW91, $\theta = {}^1/_4$	−1.63	0.026	0.151	present
periodic, PAW-RPBE, $\theta = {}^1/_4$	−1.38	0.024	0.149	25, *a*
13 atom cluster	−1.26	0.030	0.389	14, *a*
Hollow Site				
periodic, PAW-PW91, $\theta = {}^1/_4$	−1.77	−0.137	0.110	present
periodic, PAW-RPBE, $\theta = {}^1/_4$	−1.44	−0.146	0.114	25, *a*
13 atom cluster	−1.28	−0.347	0.331	14, *a*

[a] Dipole moments and polarizabilities are obtained by fitting adsorption energy vs electric field curves to eq 9.

TABLE 3: Details of PAW[32] Models Used for Linear Extrapolation of GGA Results

	cutoff radius (au)	$\Delta E_{5\sigma\text{-}2\pi^*}$ (eV)	$\Delta E_{s\text{-}t}$ (eV)
PAW hard	1.1	7.01	5.69
PAW	1.5	6.92	5.64
PAW soft	1.85	6.44	5.27

crossover of −0.198 V Å^{-1} obtained simply by displacing the curves in Figure 6b to the corrected zero-field adsorption energy. Thus, corrections to the zero field dipole moment do modify the atop vs fcc adsorption energies to some extent. However, because the dipole moments shift in the same direction and a similar amount, the point of cross-over of the two curves in Figure 6 depends mainly on the zero field difference in binding energies and not on the change in dipole moments due to extrapolation.

Vibrational Stark Effect. Vibrational spectroscopy is the most direct means to observe changes in CO adsorption with applied field. Figure 8 shows the GGA-calculated effect of electric field F on atop C−O vibrational frequency, ν_{C-O}, and bond length, r_{C-O}. Both vary nearly linearly and in opposite directions with electric field, so that a decrease in C−O bond length corresponds with an increase in vibrational frequency, in accord with Badger's rule.[42] The small curvature seen in ν versus F reflects higher order Stark effects. The Pt−C distance, r_{Pt-C}, and vibrational frequencies, ν_{Pt-C}, change in opposite

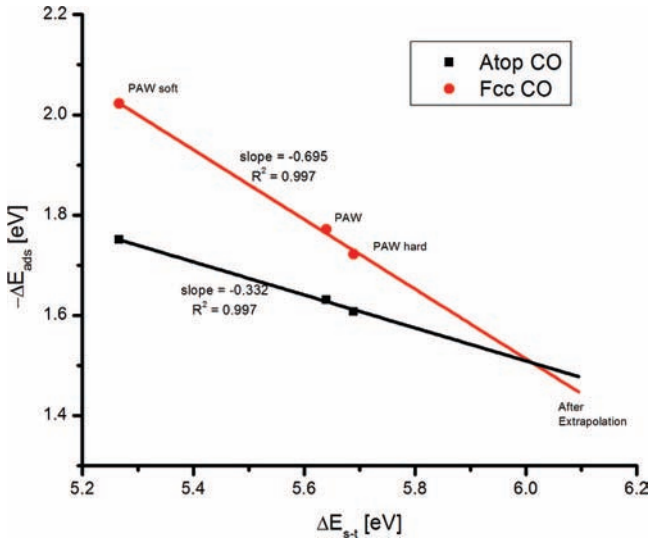

Figure 7. Linear correlation between GGA atop and fcc CO adsorption energies and gas-phase CO singlet−triplet excitation energy ($\Delta E_{s\text{-}t}$).

TABLE 4: Site-Dependent CO Adsorption Energies, Bond Lengths, Dipole Moments, and Polarizabilities from Different PAW Core Models[a]

	$\Delta E_{s\text{-}t}$ (eV)	ΔE_0 (eV)	μ_0 (e Å)	α (e Å^2 V^{-1})	r_{C-O} (Å)	dr_{C-O}/dF (Å^2 V^{-1})
Atop CO						
PAW soft	5.266	−1.751	−0.023	0.157	1.195	−0.0078
PAW	5.640	−1.631	0.026	0.151	1.157	−0.0083
PAW hard	5.689	−1.607	0.038	0.151	1.149	−0.0085
R^2		−0.997	0.991	0.990	0.998	0.975
extrapolation	6.095	−1.478	0.091	0.146	1.108	−0.0091
fcc CO						
PAW soft	5.266	−2.023	−0.180	0.113	1.232	−0.0084
PAW	5.640	−1.772	−0.137	0.110	1.191	−0.0095
PAW hard	5.689	−1.722	−0.126	0.110	1.184	−0.0100
R^2		−0.997	0.991	0.999	0.998	0.965
extrapolation	6.095	−1.447	−0.080	0.109	1.141	−0.0112

[a] The R^2 values are the correlation coefficients of the linear fits.

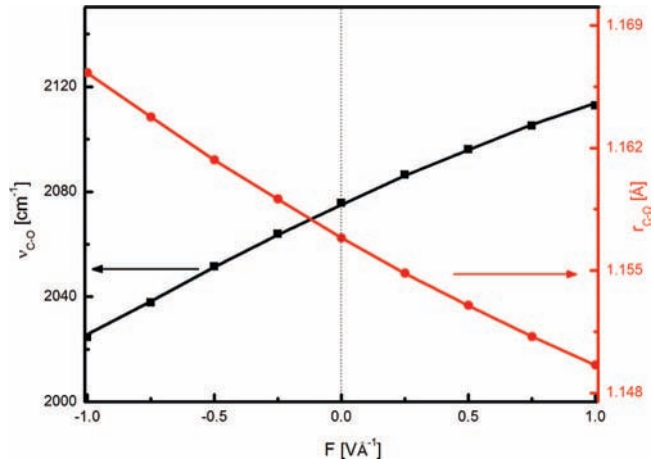

Figure 8. C−O bond length and vibrational frequency vs electric field for molecule adsorbed at atop site.

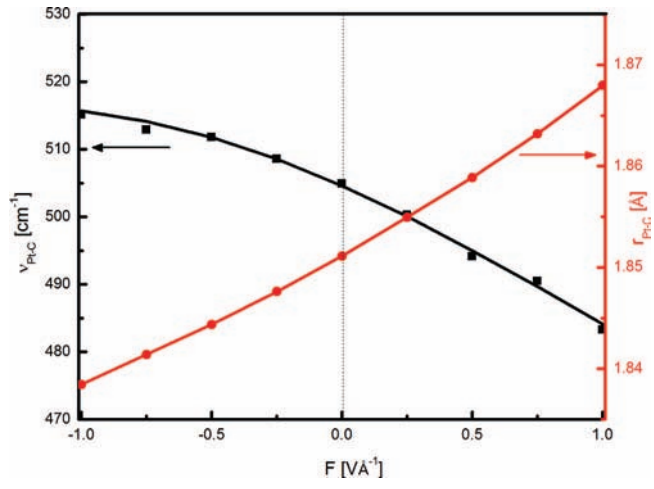

Figure 9. Pt−C bond length and vibrational frequency vs electric field for CO molecule adsorbed at atop site.

direction to that of C−O in response to the electric field (Figure 9). The slope dν_{C-O}/dF at $^1/_4$ monolayer CO coverage is 44.4 cm^{-1} V^{-1} Å, in good agreement with the 45.2 cm^{-1} V^{-1} Å value reported by Lozovoi and Alavi, calculated by applying an electric field to a three layer Pt slab at $^1/_4$ monolayer CO coverage using the method shown schematically in Figure 1c.[21] We find dν_{Pt-C}/dF is −15.8 cm^{-1} V^{-1} Å, more than 50% greater than the −9.2 cm^{-1} V^{-1} Å from these earlier calculations. The

TABLE 5: Atop CO/Pt(111) Zero Field Dipole Moment, Polarizability, and Stark Tuning Rates as a Function of Coverage

θ (monolayer)	μ_0 (e Å)	α (e Å^2 V^{-1})	$d\nu_{C-O}/dF$ (cm^{-1} V^{-1} Å)	$d\nu_{Pt-C}/dF$ (cm^{-1} V^{-1} Å)
1/12	0.031	0.176	59.57	−22.0
1/9	0.031	0.167	56.67	−21.1
1/4	0.026	0.151	44.44	−15.8

Pt−C vibrational frequency trends are somewhat noisy, which we attribute to small residual forces after the geometry optimization. Consistent with the results found here, Curulla Ferré and Niemantsverdriet[25] recently reported $d\nu_{C-O}/dF$ and $d\nu_{Pt-C}/dF$ values of +45.58 and −15.02 cm^{-1} V^{-1} Å, respectively, using a supercell model similar to that reported here but different GGA functional.

Table 5 lists the dipole moment, polarizability and Stark tuning rates at several different atop CO coverages. The Stark tuning rates decrease linearly with increasing CO coverage. At higher coverages the external field is increasingly screened from the adsorbates, leading to lower local electric field strength near the surface, as can be seen in the plane-averaged potential distribution shown in Figure 4b. The potential drop is steeper near the surface at lower coverages, in agreement with the experimental observations of Luo et al.[7] In fact, the screening factor introduced as a fitted parameter in their semiclassical model[6] can also be calculated from these electrostatic potential distributions. Figure 10 compares the coverage-dependent Stark tuning rates in this study to the values measured from UHV experiments. It can be seen that the two are in good agreement in general, although the theoretical tuning rates are slightly smaller than the experimental ones. The predicted coverage dependence is in excellent agreement with previous periodic DFT calculations.[25]

To examine the potential effect of the GGA $5\sigma-2\pi^*$ underprediction error on the Stark effect, we used the same extrapolation method as described above to obtain a corrected atop CO equilibrium bond length and its rate of change with applied field. As shown in Table 4, the zero-field CO bond length decreases on extrapolation, which suggests by Badger's rule[42] that the zero field vibrational frequency will increase, potentially moving it closer to the experimental value of 2100 cm^{-1} [43] from our uncorrected GGA value of 2076 cm^{-1}.

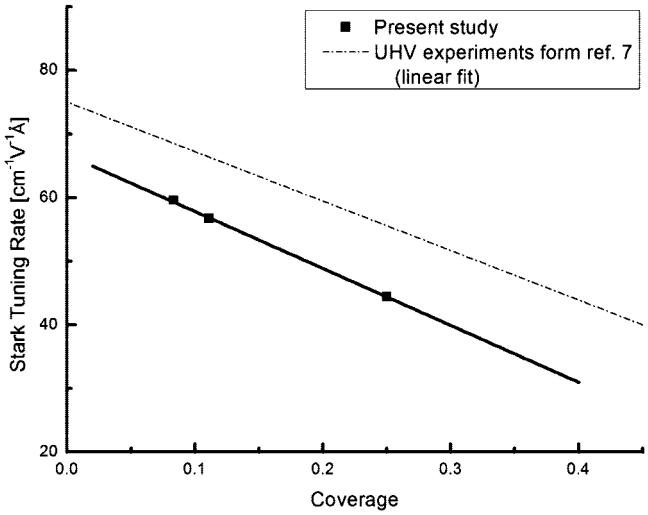

Figure 10. Rate of change of vibrational frequency with electric field (Stark tuning rate) as a function of atop CO coverage.

Following a treatment originally proposed by Lambert,[6] Wasileski et al.[44] showed that, consistent with Badger's rule, the vibrational Stark tuning rates depend linearly on the rate of change of equilibrium C−O bond length with electric field, dr_{C-O}/dF. From Table 4, we find that the extrapolated dr_{C-O}/dF increases by 9% over the uncorrected GGA value. On the basis of this trend, we expect the vibrational Stark tuning rates to also increase slightly and to move closer to the UHV experiment values[7] with this correction.

The Stark tuning rate increases for a slab in which all Pt atoms are frozen to their bulk positions. For example, at $^1/_{12}$ monolayer coverage, the tuning rate increases from 59.57 cm^{-1} V^{-1} Å for a relaxed slab to 70.62 cm^{-1} V^{-1} Å for a rigid slab. This observation in part explains the differences between Pt cluster and slab calculations of CO Stark tuning. The clusters represent a zero coverage limit, and all cluster atoms are usually fixed to their bulk metal positions. These two effects are significant, but they do not explain the whole of the discrepancy, because different cluster calculations predict tuning rates in the range of 100−120 cm^{-1} V^{-1} Å.[13,14]

Finite size effects are another factor introduced by cluster models. This effect was studied by Hymann and Medlin[16] for oxygen adsorption on Pt(111). The dipole moment of adsorbed atoms or molecules was found to converge slowly with cluster size, which effects the stabilization or destabilization of the surface dipole by an electric field (eq 7). The dipole moment did not converge even for clusters as large as 22 atoms. As a result the magnitude of the binding energy change with electric field for a 10 atom clusters at 0.51 V Å^{-1} field was found to be an order of magnitude greater than that obtained in periodic calculations. The atop CO dipole moment is not very different in periodic and cluster calculations because charge transfer is slight between surface and adsorbate. However, the atop CO polarizability is much larger in the cluster calculations, as seen in Table 2, which accounts for the larger binding energy sensitivity to applied field. Stark tuning rates are sensitive to derivatives of dipole moment and polarizability with respect to bond length[44] and differences in each will contribute to differences between slab and cluster predicted Stark tuning rates.

Conclusions

In this work, we report supercell DFT-GGA calculations of the equilibrium geometry, dipole moment, adsorption energy, and stretching vibrational frequencies of CO adsorbed atop and fcc on Pt(111) as a function of external electric field, including corrections to the GGA site-preference error.[29] External electric fields redistribute charge into or away from adsorbed CO and cause a change its dipole moment. The electric field effect can be quantified by the calculated zero field adsorbate dipole moment and polarizability. Different supercell calculations[25] predict similar values of dipole moment and polarizability, whereas cluster calculations[14] predict a significantly different dipole moment and a much higher polarizability.

Analysis of changes in charge and electrostatic potential distribution show that an applied electric field is screened near the adsorbate. This screening effect is coverage dependent, leading to a coverage dependence of the shifts in binding energy and vibrational frequencies (Stark tuning rate). The Stark tuning rates for C−O and Pt−C stretch frequencies at $^1/_4$ monolayer coverage obtained in this study are +44.4 and −15.8 cm^{-1} V^{-1} Å, respectively. The former value is in good agreement with periodic DFT calculations,[21] and slightly smaller than that obtained from UHV experiments, 56 cm^{-1} V^{-1} Å.[7] The coverage dependence of tuning rates is in good agreement with UHV experiments and other calculations.[25]

The results here indicate that atop and fcc CO binding energies respond differently to applied fields, and that changes in binding energy in fields of ± 1 V Å^{-1} are in the range 0.1−0.15 eV. The change, though small, can have a significant effect on the thermodynamics and kinetics of CO adsorption and reaction on Pt, for example, by changing the preferred adsorption site from atop to hollow. Moreover, the basic concepts from this study can be applied to a number of other systems with potentially interesting electric field effects. The relative magnitude of the field effect on CO binding will be greater on metal surfaces on which CO binds less strongly. Different adsorbates with higher static dipole moments and polarizabilities and different electron withdrawing or donating behavior can also exhibit stronger electric field effects, as observed in the cluster calculations of Wasileski et al.[15] Transition-state energies can also exhibit relatively larger effects, as observed for O_2 dissociation[16] and some other reactions,[8] thus significantly affecting the rates of reactions. Thus, more detailed calculations need to be done to improve our understanding of not only electrochemical systems but also the electronic effects of promoters and catalyst supports in heterogeneous catalysis. The effect of electric fields at the junction of Pt catalyst on semiconducting TiO_2 support is being investigated experimentally in our laboratory using electrical measurements and infrared spectroscopic studies of chemisorption on nanofabricated catalytic junctions.[45]

Acknowledgment. Financial support from NSF grant 0854324 and computing resources provided by the University of Notre Dame Center for Research Computing are gratefully acknowledged.

References and Notes

(1) van Santen, R. A.; Neurock, M. *Catal. Rev.: Sci. Eng.* **1995**, *37*, 557.
(2) Feibelman, P. J.; Hammer, B.; Nørskov, J. K.; Wagner, F.; Scheffler, M.; Stumpf, R.; Watwe, R.; Dumesic, J. A. *J. Phys. Chem. B* **2001**, *105*, 4018.
(3) Koper, M. T. M.; van Santen, R. A.; Wasileski, S. A.; Weaver, M. J. *J. Chem. Phys.* **2000**, *113*, 4392.
(4) Weaver, M. J.; Zou, S.; Tang, C. *J. Chem. Phys.* **1999**, *111*, 368.
(5) Lambert, D. K. *Electrochim. Acta* **1996**, *41*, 623.
(6) Lambert, D. K. *J. Chem. Phys.* **1988**, *89*, 3847.
(7) Luo, J. S.; Tobin, R. G.; Lambert, D. K. *Chem. Phys. Lett.* **1993**, *204*, 445.
(8) Pacchioni, G.; Lomas, J. R.; Illas, F. *J. Mol. Catal. A, Chem.* **1997**, *119*, 263.
(9) Linic, S.; Barteau, M. A. *J. Am. Chem. Soc.* **2004**, *126*, 8086.
(10) Schwab, G. M. *Adv. Catal.* **1978**, *27*, 1–22.
(11) Hayek, K.; Kramer, R.; Paal, Z. *Appl. Catal. a-General* **1997**, *162*, 1–15.
(12) Jochum, W.; Eder, D.; Kaltenhauser, G.; Kramer, R. *Top. Catal.* **2007**, *46*, 49–55.
(13) Wasileski, S. A.; Weaver, M. J.; Koper, M. T. M. *J. Electroanal. Chem.* **2001**, *500*, 344.
(14) Wasileski, S. A.; Koper, M. T. M.; Weaver, M. J. *J. Phys. Chem. B* **2001**, *105*, 3518–3530.
(15) Wasileski, S. A.; Koper, M. T. M.; Weaver, M. J. *J. Am. Chem. Soc.* **2002**, *124*, 2796.
(16) Hyman, M. P.; Medlin, J. W. *J. Phys. Chem. B* **2005**, *109*, 6304–6310.
(17) Wasileski, S. A.; Weaver, M. J. *J. Phys. Chem. B* **2002**, *106*, 4782.
(18) Lozovoi, A. Y.; Alavi, A.; Kohanoff, J.; Lyden-Bell, R. M. *J. Chem. Phys.* **2001**, *115*, 1661.
(19) Taylor, C. D.; Wasileski, S. A.; Filhol, J. S.; Neurock, M. *Phys. Rev. B* **2006**, *73*, 165402.
(20) Lozovoi, A. Y.; Alavi, A. *Phys. Rev. B* **2003**, *68*, 245416.
(21) Lozovoi, A. Y.; Alavi, A. *J. Electroanal. Chem.* **2007**, *607*, 140–146.
(22) He, Y.; Wei, X. Y.; Chan, C. T.; Che, J. G. *Phys. Rev. B* **2005**, *71*, 45401.
(23) Neugebauer, J.; Scheffler, M. *Phys. Rev. B* **1992**, *46*, 16067–16080.
(24) Feibelman, P. J. *Phys. Rev. B* **2001**, *6412*.
(25) Curulla Ferré, D.; Niemantsverdriet, J. W. *Electrochim. Acta* **2008**, *53*, 2897.
(26) Hammer, B.; Hansen, J. B.; Nørskov, J. K. *Phys. Rev. B, Condensed Matter* **1999**, *59*, 7413.
(27) Gil, A.; Clotet, A.; Ricart, J. M.; Kresse, G.; García-Hernández, M.; Rösch, N.; Sautet, P. *Surf. Sci.* **2003**, *530*, 71.
(28) Kresse, G.; Gil, A.; Sautet, P. *Phys. Rev. B, Condensed Matter* **2003**, *68*, 73401.
(29) Mason, S. E.; Grinberg, I.; Rappe, A. M. *Phys. Rev. B, Condensed Matter* **2004**, *69*, 161401.
(30) Kresse, G.; Furthmuller, J. *Comput. Mater. Sci.* **1996**, *6*, 15–50.
(31) Blochl, P. E. *Phys. Rev. B* **1994**, *50*, 17953–17979.
(32) Kresse, G.; Joubert, D. *Phys. Rev. B* **1999**, *59*, 1758–1775.
(33) Perdew, J. P.; Chevary, J. A.; Vosko, S. H.; Jackson, K. A.; Pederson, M. R.; Singh, D. J.; Fiolhais, C. *Phys. Rev. B* **1992**, *46*, 6671–6687.
(34) Perdew, J. P.; Wang, Y. *Phys. Rev. B* **1992**, *45*, 13244–13249.
(35) Monkhorst, H. J.; Pack, J. D. *Phys. Rev. B* **1976**, *13*, 5188.
(36) Kittel, C. *Introduction to Solid State Physics*; John Wiley & Sons Inc.: New York, 1996.
(37) Foiles, S. M.; Baskes, M. I.; Daw, M. S. *Phys. Rev. B* **1986**, *33*, 7983.
(38) Gilliam, O. R.; Johnson, C. M.; Gordy, W. *Phys. Rev. (Ser. I and II)* **1950**, *78*, 140.
(39) Muenter, J. S. *J. Mol. Spectrosc.* **1975**, *55*, 490.
(40) Blyholder, G. *J. Phys. Chem.* **1964**, *68*, 2772.
(41) Herzberg, G. *In Electronic spectra and electronic structure of polyatomic molecules: v. 3: Molecular Spectra and Molecular Structure*; Van Nostrand Reinhold: 1966.
(42) Cioslowski, J.; Liu, G.; Mosquera Castro, R. A. *Chem. Phys. Lett.* **2000**, *331*, 497.
(43) Gajdoš, M.; Eichler, A.; Hafner, J. *J. Phys.: Condens. Matter* **2004**, *16*, 1141.
(44) Wasileski, S. A.; Koper, M. T. M.; Weaver, M. J. *J. Chem. Phys.* **2001**, *115*, 8193.
(45) Deshlahra, P.; Wolf, E. E. Abstract submitted to 21st North American Catalysis Society Meeting, 2009.
(46) Curulla, D.; Clotet, A.; Ricart, J. M.; Illas, F. *J. Phys. Chem. B* **1999**, *103*, 5246.
(47) Xu, Y.; Getman, R. B.; Shelton, W. A.; Schneider, W. F. *Phys. Chem. Chem. Phys.* **2008**, *10*, 6009.
(48) Hammer, B.; Morikawa, Y.; Nørskov, J. K. *Phys. Rev. Lett.* **1996**, *76*, 2141.

JP810518X